J Mater Sci: Mater Electron (2015) 26:791–800
DOI 10.1007/s10854-014-2465-2

Characterization and optoelectronics investigations of mixed donor ligand directed semiconductor ZnO nanoparticles

Charu Narula · Inderpreet Kaur · Navneet Kaur

Received: 29 August 2014 / Accepted: 28 October 2014 / Published online: 11 November 2014

Abstract The optical properties of mixed donor ligand directed semiconductor ZnO nanoparticles are evaluated and imine linked receptor is used as capping agents. The ZnO nanoparticles are prepared using precipitation method. The ligand is synthesized using condensation reaction between 2-aminothiophenol and 2-thiophenecarboxaldehyde. The formation of ligand is confirmed with spectroscopic methods including NMR and mass spectroscopy. However, UV–Vis absorption, photoluminescence, X-ray diffraction, energy dispersive X-ray and FTIR spectroscopy techniques are used for characterization of the ligand coated ZnO nanoparticles. The capping with ligand resulted in the successful amendment of the surface of ZnO nanoparticles, as it particularly reduced the defects related visible emission known as green luminescence and hence resulted in improvement in the UV luminescence. The UV–Vis absorption spectra also showed blue shift in the UV region for the ligand based ZnO nanoparticles due to the effect of quantum confinement. The composite (ZnO-ligands) stability is confirmed theoretically with Density Functional Theory.

C. Narula · N. Kaur (✉)
Centre for Nanoscience and Nanotechnology (UIEAST), Panjab University, Chandigarh 160014, India
e-mail: navneetkaur@pu.ac.in

I. Kaur
Biomolecular Electronics and Nanotechnology Division (BEND), Central Scientific Instruments Organization (CSIO), Chandigarh 160030, India

1 Introduction

Nanoparticles are gaining much of the attentions because of their unique physical, chemical, electrical and optical properties in comparison to their bulk counterpart due to the exciton confinement [1–4]. The impact of excitonic effects is more prominent in Quantum Dots. A strong difference is observed in optical absorption, exciton energies and electron–hole pair recombination for QDs with particle size $<\sim 30$ nm [5]. Accordingly, researchers are expecting much of the use of QDs in optoelectronic applications. The blue shift in the emission wavelength and increase in the emission efficiency can be realized in case of QDs because of carrier confinement effects and hence QDs can be used for the fabrication of light emitting diodes [6–10]. The QDs can also find its application in down conversion of ultraviolet light from inorganic LEDs [11–16]. Since the absorption of QDs can be tuned from Ultraviolet to the visible region the QDs can be used for the fabrication of sensitized solar cell [17–21]. The high quantum yield (QY), high extinction coefficient, narrow emission peaks, size tunable absorbance and emission of QDs leads to its use in Bioimaging applications [22–24]. The optical absorption, quantum efficiency, luminescence intensity and spectrum of QDs are strongly dependent on surface states [25] because the energy of the surface states lie in the band gap of the QDs [26]. Surface passivation can enhance the photostability of QDs [5].

The wurtzite semiconductor Zinc Oxide has got a lot of interest in research community because of its direct wide band gap of 3.37 eV and high exciton binding energy (60 meV) [27]. It has attracted concentrated research because of its unique properties. Zinc oxide semiconductor is blessed with several favorable properties such as high electron mobility, transparency, strong room temperature

luminescence, high electrochemical stability, control over resistance (10^{-3}–10^{-5} Ω) etc. The ZnO QDs have size dependent electrical and optical properties. Zinc Oxide QDs are excellent applicants for solar cells [28, 29], light emitting diodes [30], UV lasers, transparent UV protection films, transparent conducting oxide, transistors and gas sensors [31–35] etc. In addition to the stability, ZnO is also safe for human beings and animals [36, 37].

The morphological characteristics such as size, structure, and surface defects play a significant role on the optoelectronic properties. The large surface area of the nanoparticles results in high density of surface defects which finally control the luminescence properties. The function of the devices at molecular level can be examined by luminescence emission efficiency, which varies with the size of nanoparticles [38]. The improvement of luminous efficiency is still a major challenge to the researchers. The luminescence spectrum of ZnO nanoparticles is dominated by visible region as it shows high emission intensity in comparison to the intensity of UV region. The recombination of holes from the valence band and electrons from the conduction band results in UV emission band, but the origin of visible emission is controversial [39]. This is owed to the surface defects and a number of acceptor and donor pairs created during synthesis. The defect and impurities result in electronic levels within the band gap which results in various electronic transitions arbitrated by these levels and thus the optical band gap energy varies [40]. The defect ionization energies range from ~0.05 to 2.8 eV [41, 42]. Also the defects both intrinsic and extrinsic results in the emergence of luminescence at unusual emission wavelengths in the visible range for the excitation with the photon energy greater than band gap [43]. The concentration of surface states on the QDs is a function of passivation process. Mainly the defect emission in ZnO nanoparticles is green emission at ~540 nm [44–49]. The most widely accepted mechanism for green emission from ZnO is the electron hole recombination on singly ionized oxygen vacancies [5]. The passivation of both radiative and non-radiative recombination sites on the surface of nanoparticle can be carried out by surface modification.

The research on the optical, electronic and structural properties of ZnO nanoparticles is important for their use as optoelectronic devices in UV range. In this research paper, the effect of mixed donor ligand on the surface of ZnO nanoparticles together with its optoelectronic properties is reported. The mix ligand is synthesized in dry methanol by condensation reaction. ZnO nanoparticles capped with the ligands are synthesized by precipitation process. The functional group of the compound is confirmed by FTIR, ^{1}H-NMR and further studies for its band gap calculation with UV–Vis Spectroscopy are reported. The composite (ZnO-ligands) stability is confirmed theoretically with Density Functional Theory. Lastly, the optoelectronic characteristics are studied with Photoluminescence spectroscopy.

2 Experimental details

2.1 Materials and methods

All the chemicals used in this study were of analytical grade and they were used as such without further purification. The ^{1}H NMR spectra of organic ligand and ZnO coated with ligand were recorded on a JNM-ECS400 (JEOl) NMR spectrophotometer at 400 MHz. The absorption studies were carried out using UV–Vis spectrophotometer (Shimadzu, Japan) operating between the ranges of 200- 700 nm. Perkin Elmer LS5 fluorescence spectrophotometer was used for the fluorescence measurements with scanning speed 400 scans per second. The elemental and morphology analysis were carried out with scanning electron microscope (SEM JEOL JSM-6610LV) at 15 kV voltage. The functional groups were confirmed by FTIR spectrometer (Thermo Fisher Scientific Inc., USA). The particle size was determined using a Metrohm Microtrac Ultra Nanotrac particle size analyzer using DMSO/H_2O (8:2, v/v) system as the dispersion medium. TEM images were recorded on Hitachi instrument (H-7500) at 100 kV.

2.2 Synthesis of mixed donor ligand

The ligand **1** was synthesized by stirring the solution of 2-aminothiophenol (1.07 ml, 10 mmol) and 2-thiophenecarboxaldehyde (0.934 ml, 10.0 mmol) in dry methanol CH_3OH (30 ml) under O_2 and basic conditions (Scheme 1). The precipitates were then filtered and washed with methanol to get rid of all impurities and contaminations. The resulting fine particles were then dried over 30 h.

2.3 Synthesis of mixed donor ligand directed ZnO nanoparticles

In the final stage of synthesis, the quantum sized ZnO nanoparticles (Scheme 2) were prepared in a round bottom flask by taking $Zn(NO_3)_2.6H_2O$ (0.221 g, 0.744 mmol) along with a mixed donor ligand (0.650 g, 1.4887 mmol). The NaOH solution was then added drop-wise to the above solution using dropping funnel. The solution was then stirred in an ultrasonic bath for 3 h and a dispersion of ZnO particles were gradually formed in the solution. The as-prepared dispersion of solution was centrifugally filtered and washed with methanol several times. The product was dried at 40 °C for 24 h.

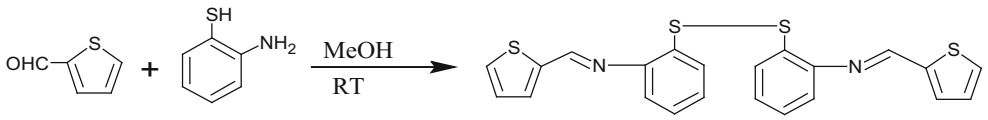

Scheme 1 Synthesis of ligand **1**

Scheme 2 Quantum sized ZnO nanoparticle capped with ligand **1**

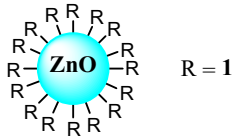

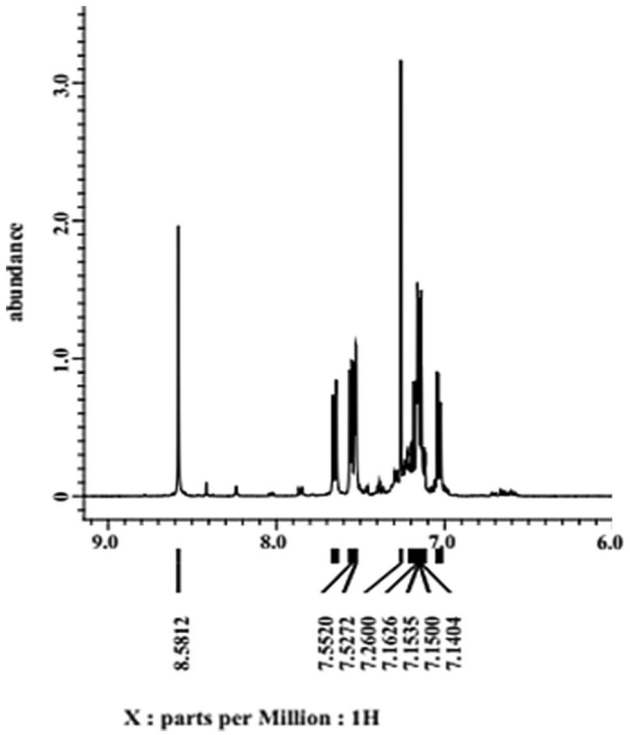

Fig. 1 ^{1}H NMR of the ligand **1**

3 Results and discussion

3.1 Characterization of organic ligand

The ligand was fully characterized by ^{1}H NMR and mass spectrum. ^{1}H NMR (400 MHz, $CDCl_3$) δ: 7.04 (d, 2H, ArH), 7.15(m, 6H, ArH), 7.53 (d, 2H, ArH), 7.56 (d, 2H, ArH), 7.64 (d, 2H, ArH), 8.58 (s. 2H, –CH=N) Fig. 1. The ligand was further characterized by mass spectroscopic technique ESI–MS, which shows m/z = 437.3 $[M + H]^{+}$, where M = $C_{22}H_{16}N_2S_4$ (Fig. 2). DFT calculations of the ligand were performed using GGA–DFT package of DMol3. Figure 3 represents ball and stick model of the ligand. Optimized structure of the ligand with distribution of LUMO and HOMO is also shown in Fig. 4. Clearly, the LUMO densities are mainly concentrated on thiophene rings and C=N group with energy −3.549 eV and HOMO densities are mainly concentrated on the S–S bond and thiophenol ring.

3.2 Characterization of mixed donor ligand directed ZnO nanoparticles

The quantum sized ZnO nanoparticles were characterized by ^{1}H NMR and the purity of sample was established with elemental analysis. The ^{1}H NMR (Fig. 5) shows the split in the Schiff base peak. The doublets and the triplets get merged which absolutely confirm the layer of organic ligand on the surface of ZnO. In addition, both sides of the molecule are differently linked which indicates that asymmetry has been formed. The morphology of quantum sized ZnO nanoparticles was realized with SEM (Fig. 6). The SEM image shows that modified ZnO nanoparticles form supramolecular self-assembled structures due to the structure directing nature of compound. The EDAX analysis also shows the existence of organic compounds together with ZnO (Fig. 7). This confirmed that the organic ligand 1 is successfully coated over ZnO metal oxide semiconductor. The distribution of particle size of organic ligand directed ZnO nanoparticles (1.ZnO), showing average particle size of 50 nm, was measured with DLS based particle size analyzer (Fig. 9) by dissolving the compound in DMSO: H_2O (70:30; v/v). DLS is showing somewhat larger particle size as compared to TEM (Fig. 8) analysis due to hydro-dynamic radius of nano-aggregates during DLS analysis.

3.3 FTIR analyses of mixed donor ligand directed ZnO nanoparticles

The quantum sized ZnO nanoparticles were further characterized by FTIR spectrum (Fig. 10). The FTIR spectrum for the uncapped ZnO resulted in no characteristic functional group in the region of lower frequencies apart from some very weak absorption around 3,500 and 1,600 cm^{-1} [50], whereas a series of absorption peaks ranging from 500 to 4,000 cm^{-1} can be found in capped ZnO nanoparticles, which is due to the existence of organic groups and chemisorbed species in mixed donor ligand based ZnO nanoparticle surface. Band around 1,500 to 1,600 cm^{-1}

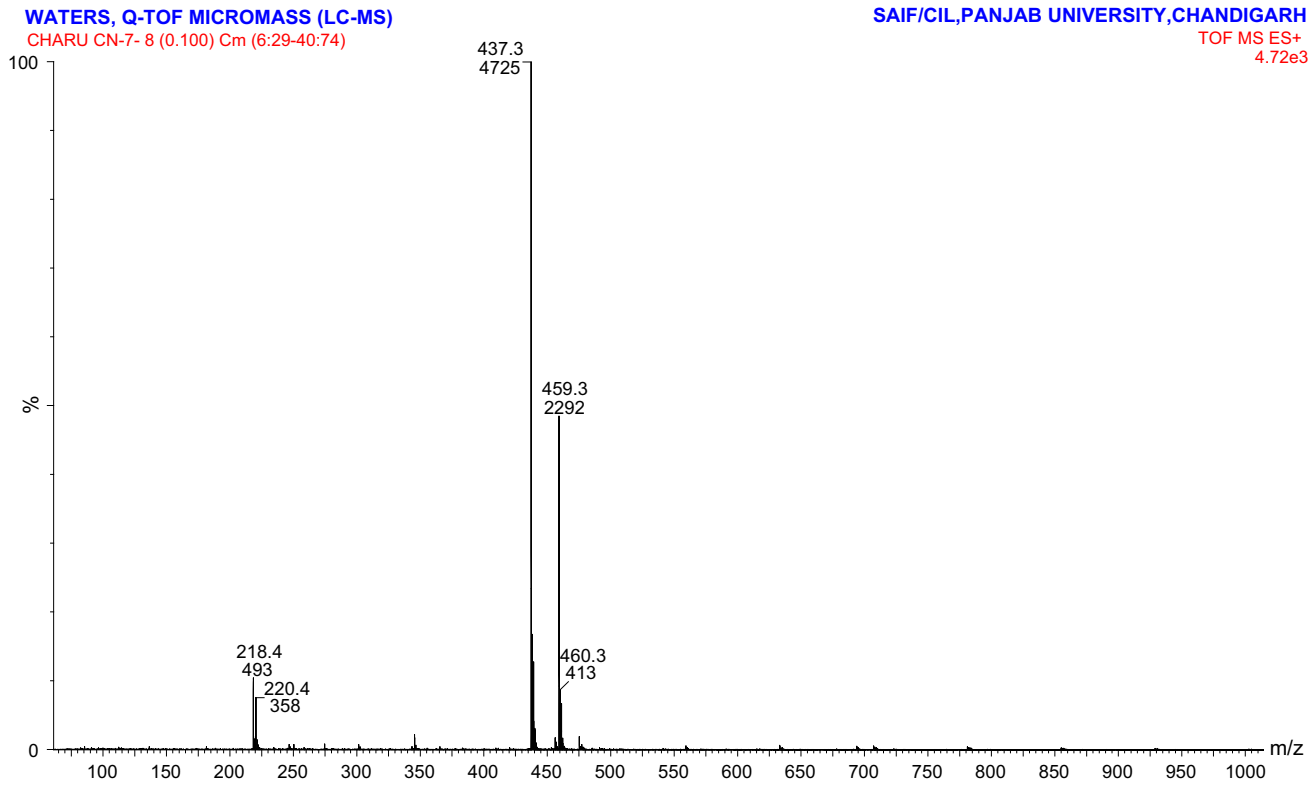

Fig. 2 Mass spectrum of the ligand **1**

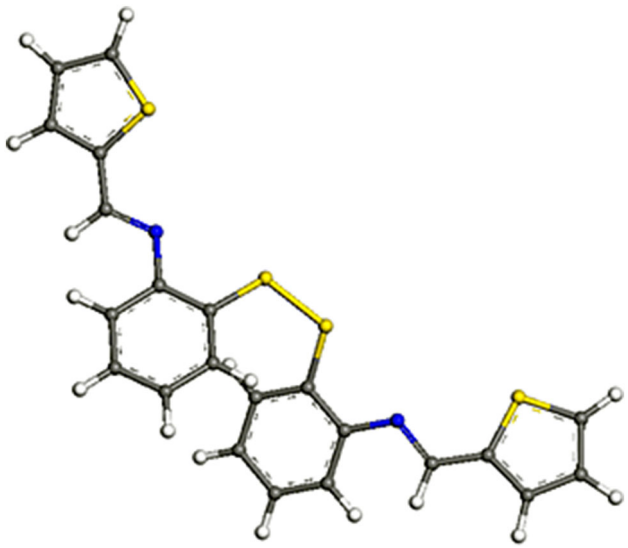

Fig. 3 DFT optimized structure of the ligand **1**

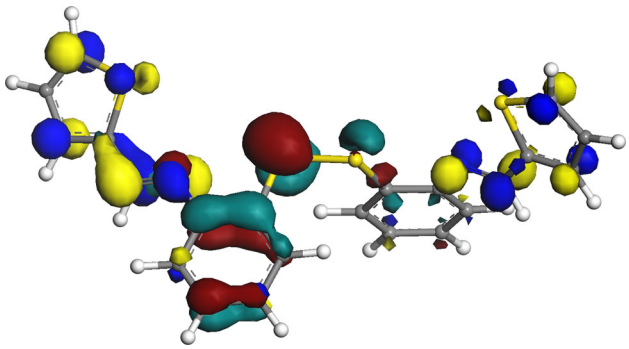

Fig. 4 Distribution of HOMO and LUMO **1**

shows the vibration of C=N group of ligand. The presence of peaks at 1,384 and 1,422 cm^{-1} corresponds to C–C stretch of aromatic ring. Finally, the peaks around 724 cm^{-1} represents S–S linkage and those at 750 cm^{-1} are due to the C–H group of Schiff base. Hence, the FTIR analyses confirmed the presence of mixed donor ligand.

3.4 DFT calculations to study the interaction of mixed donor ligand on ZnO

DFT calculations were performed to understand the interaction of mixed donor ligand on ZnO. The ZnO nanoparticles are represented by a small cluster $(ZnO)_5$. The DFT optimized geometries of ZnO, organic ligand and $(ZnO)_5$ with organic ligand shown in Fig. 11a–c respectively were

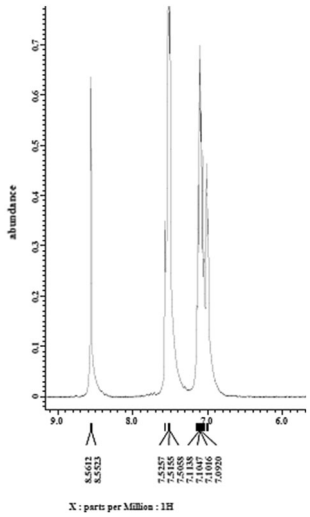

Fig. 5 ^{1}H NMR of ZnO capped with mixed donor ligand (1.ZnO)

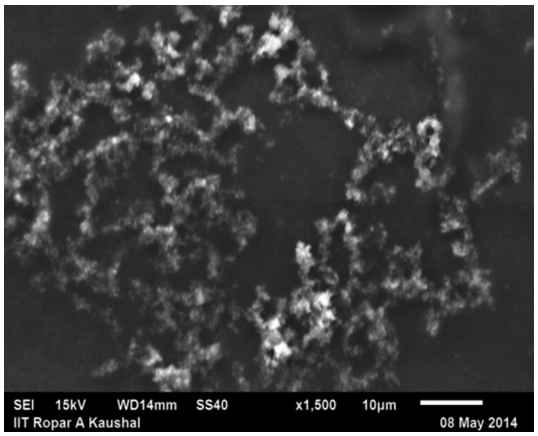

Fig. 6 SEM image of 1.ZnO showing self assembled structure

obtained by using B3LYP/6-311G basis set on Gaussian 03 program. The optimized ligand represents a symmetrical structure with both side arms parallel to each other. A clear change in the structure of ligand was noticed (Fig. 11c) when ZnO was taken along with organic ligand. Both arms of the ligand which were initially parallel to each other in the absence of $(ZnO)_5$, now has become perpendicular. It also authenticated the result obtained from ^{1}H NMR, which showed split in Schiff base peak when ZnO was coated with mixed donor ligand (Fig. 5). This may happened because of the attraction felt by oxygen of ZnO towards the hydrogen of thiophene ring forming a capping monolayer. This resulted in asymmetrical structure as both arms were differently linked. The energy of optimization also showed that a small $(ZnO)_5$ cluster with ligand has more stability as compared to isolated mixed donor ligand (Table 1).

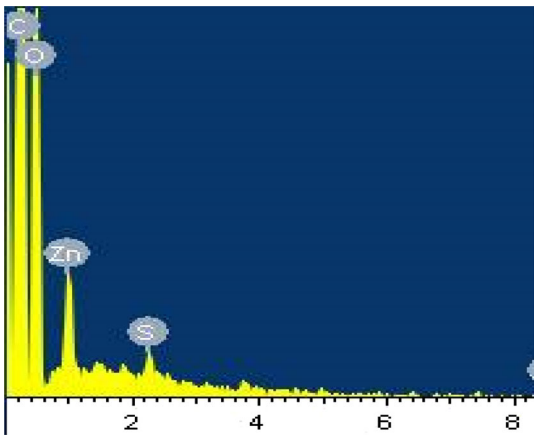

Fig. 7 EDAX analysis of 1.ZnO showing the existence of organic compound together with ZnO

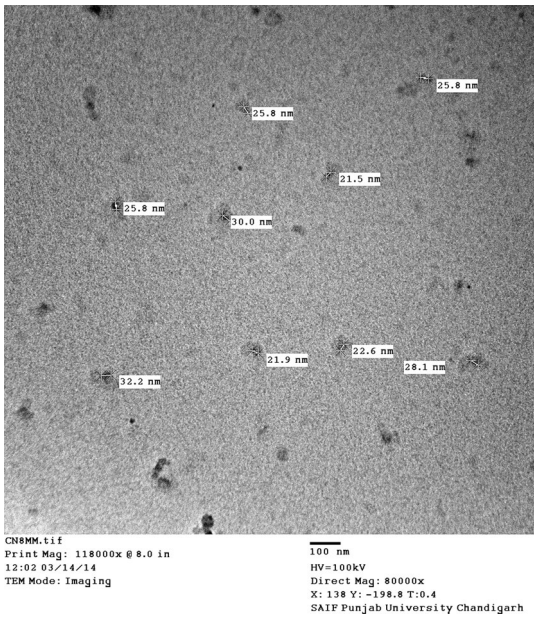

Fig. 8 TEM image of 1.ZnO showing average size 25 nm

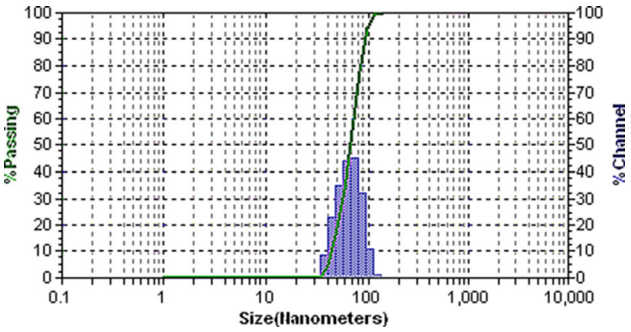

Fig. 9 DLS based particle size analyzer showing particle size of 50 nm

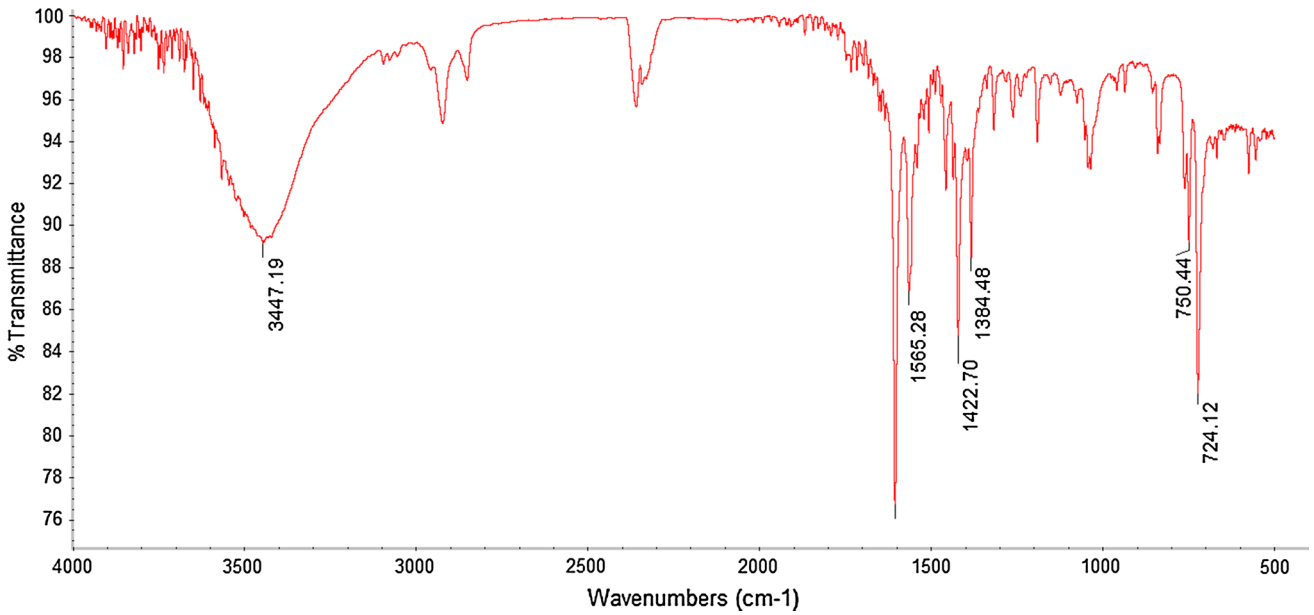

Fig. 10 FTIR spectrum of mixed donor ligand directed ZnO nanoparticles (1.ZnO)

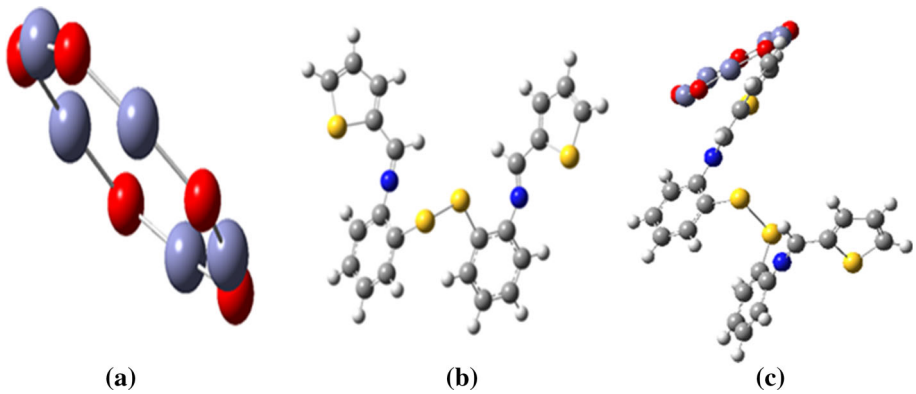

Fig. 11 **a** Optimized $(ZnO)_5$ cluster, **b** optimized organic ligand showing both side group arms parallel to each other, **c** ZnO along with organic ligand showing one side group attracted towards ZnO, while the other left unreacted

Table 1 The optimization parameters of ZnO, organic ligand and ZnO with ligand calculated at B3LYP/6-311G level

	Energy (a.u.)
ZnO	−9,272.73 a.u.
Organic ligand 1	−2,550.040 a.u.
ZnO with organic ligand (1.ZnO)	−11,822.864 a.u.

3.5 Capping mechanism of mixed donor ligand directed ZnO nanoparticles

The semiconductor nanoparticles are extensively used in optoelectronics as they have very fascinating size dependent optical properties. As the size of semiconductor nanoparticle approaches Bohr exciton radius, blue shift is observed in the emission and absorption spectra [51]. An important requirement for the device applications in the UV range is augmentation of NBE luminous intensity with a cut in the emission intensity in visible region. The UV emission intensity can be improved only if the visible emission (defect related) could be censored. The luminescence properties of metal oxide semiconductor ZnO nanoparticles can be improved when their surface gets capped. A capping agent is a strongly absorbed monolayer of usually organic molecules used to aid stabilization of nanoparticles. The capping agent efficiently manages the size of the particle by restricting the particle growth even after nucleation stage. The surface structure of the ZnO nanoparticles changes, when the nanoparticle surface chemically reacts with the modifier (capping agent). The bonding between the nanoparticle surface and the modifier decreases the force of OH^- ions present on the surface. So the hydrogen bonding between the nanoparticles gets eradicated which finally prevents the oxygen bride bonding [52]. It is observed that polymer materials or organic

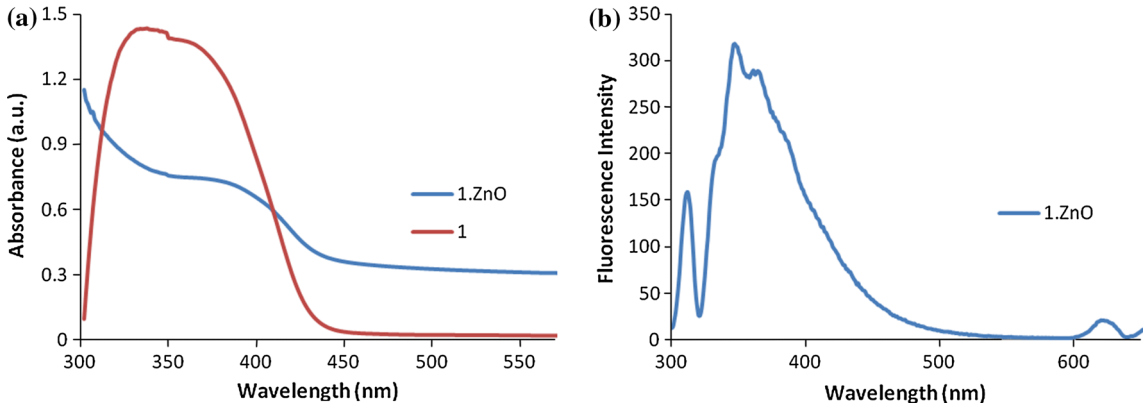

Fig. 12 **a** A comparison of solid state UV–Vis absorption spectra of both 1 and 1.ZnO and **b** PL spectra of ligand directed 1.ZnO nanoparticles

receptors are good capping agents for ZnO nanoparticles, which can efficiently passivate the surface defects and thus reduces the surface-related visible emission [52–55]. The ligand here is used to manage the size of nanoparticles by controlling the expansion process. The ligand is used to shield the ZnO nanoparticles from aggregation and thus improves the optoelectronic properties of the nanoparticles as the surface defects were reduced [56]. Also since the asymmetry is formed (as clear from both ^{1}H NMR and DFT studies), one group would have reacted with the OH^{-} group on the ZnO surface which lead to the capping monolayer, while the unreacted side group stick to the surface resulting in encouraging stability of the surface.

3.6 Photoluminescence (PL) and UV–Vis absorption studies of mixed donor ligand directed ZnO nanoparticles

Nanoparticles, in general, have two excitations: excitonic transitions and deep level transitions. The excitonic transitions are the result of transition from conduction band to valence band and deep level transitions are caused by the surface defects that appear as the size of nanoparticle reduces. ZnO nanoparticles capped with an organic receptor were examined by UV–Vis absorption spectroscopic and photoluminescence (PL) techniques. A comparison of solid state UV–Vis absorption spectra of organic ligand (1) and ZnO coated with ligand (1.ZnO) is shown in Fig. 12a.

The ligand 1 exhibited peak at 348 nm, where as the ZnO (pure) exhibits peak at 380 nm corresponding to exciton state of ZnO [57]. So the ligand 1 which acts as capping agent on ZnO and turned into 1.ZnO, resulted in blue shift in the absorption spectra, and hence the band gap is increased. The probable reason behind this phenomenon is strong quantum confinement effects. The radiative absorption in 345-365 nm range may be attributed to the interband absorptions taking place among the remotely segregated discrete energy states of conduction and valence band. The existence of discrete energy states and the consequent blue shift in absorption energy are the signs of quantum size confinement in ZnO nanoparticles [58]. As the size of particle reduces, the continuity observed in the conduction band and valence band (in case of bulk materials) is converted to discrete energy levels. In the prepared ZnO nanoparticles, a number of such discrete energy states are found probably due to two causes. First, due to large surface to volume ratio of nanoparticles and/or defect states (viz. vacancy, interstitial, antisites of zinc or oxygen) that may appear due to excess oxygen in the prepared ZnO nanoparticles. And secondly, the definite band structure analogous to each finite sized nanoparticle, where discrete far spaced energy states are available [58]. As evident from TEM (Fig. 8), the prepared ZnO nanoparticles have size distribution of the order of 25–30 nm, due to which different band structures and energy states would be obtained. Hence, in the formed oxygen rich ZnO nanoparticles, discrete energy states for conduction and valence band region emerge along with the defect states within the mentioned region. The PL spectra of ZnO nanoparticles shows a near band edge UV region accompanied by the broad defect associated visible region. The visible emission is generally green luminescence with the existence of other emissions such as blue, yellow and bluish-yellow luminescence in the PL spectra. For various device applications such as UV laser, it is essential to suppress the visible emission in the PL spectra. Figure 12b shows the room temperature PL spectra of ZnO capped with an organic receptor excited with 306 nm wavelength. The PL data was recorded in the range of 300–650 nm. The Photoluminescence spectra demonstrated a notable decrease in visible emission intensity for the capped ZnO nanoparticles (with an organic receptor) Fig. 12b, demonstrating that defect states and the dangling bonds available on the surface of ZnO

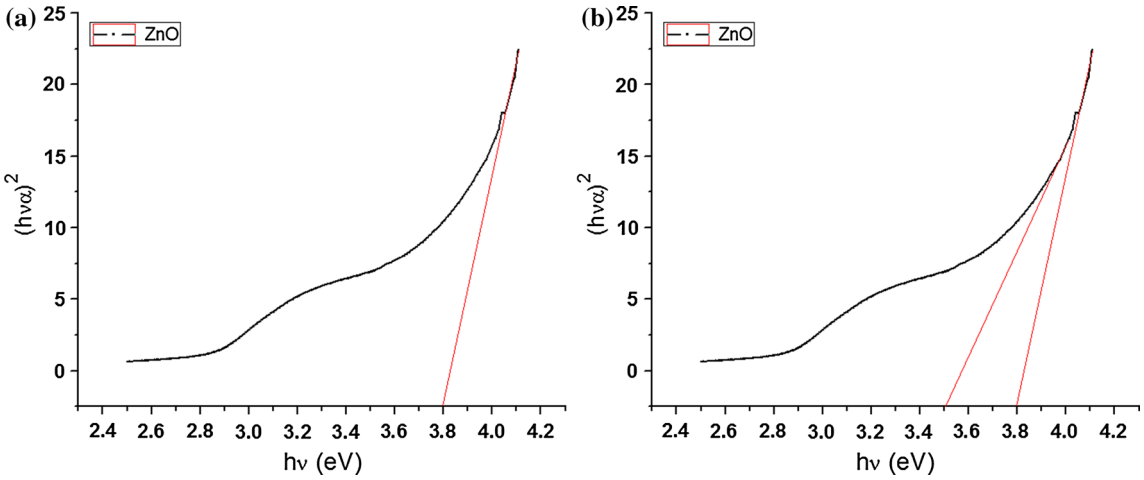

Fig. 13 **a** Band gap of 1.ZnO nanoparticles calculated as 3.8 eV using Tauc plot. **b** An approximate band gap range from 3.5 to 3.8 eV because of different particle size (25–30 nm) of synthesized nanoparticles

nanoparticles were appreciably passivated. The emission spectra from the excitonic level (347 nm) did not show any shift and is in agreement with the UV–Vis absorption observed earlier at 348 nm. A green emission band at 576 nm was observed in the fluorescence spectrum of pure ZnO [57] but its intensity get quenched after capping of ZnO with ligand 1 (Fig. 12b). PL quenching in the ZnO nanoparticles is a positive indication of the excitation dissociation intensity. The reason behind green emission may be the transition of ZnO nanoparticles from conduction band to different levels of excited impurity atoms in the ZnO band gap [59, 60] and recombination of a photo-generated hole with a single ionized electron in the valence band [61]. Dijken et al. [39] presented a model in which it was demonstrated that the surface defects decreased after capping with compound 1 and thus the emission at the visible region quenched. Moreover, the intensity of UV region increased when the surface of the ZnO nanoparticles made inert with possible capping agents. Recently, Cao et al. [62] also found that there is an increase in UV and visible emission intensities of ZnS:Mn^{2+}/ZnO with passivation. In ZnO nanoparticles, the non-radiative processes are also caused by the surface states such as dangling bonds. Therefore, the reduction of the dangling bonds of ZnO nanoparticles after capping may result in the increase in the UV emission intensity.

The band gap of pure ZnO nanoparticles as reported in the literature [63] is 3.37 eV. The band gap of any material is its size dependent property. We have calculated the band gap of ZnO coated with Schiff reagent from its molar absorptivity obtained from UV–Vis spectroscopic analysis. The coated ZnO nanoparticles was investigated by calculating band gap (E_g), using Tauc Plot Equation given below.

$$Ahv = A\,(hv - E_g)^{1/2} \quad (1)$$

where A is Absorbance, h is Planck's constant, v is frequency and E_g is the band gap.

The band gap of the mixed donor ligand directed ZnO nanoparticles was calculated as 3.8 eV (Fig. 13a) which is higher than the uncapped ZnO nanoparticles. The increase in the band gap of ligand directed ZnO nanoparticles also infer the reduction in the size of the synthesized mixed donor ligand directed ZnO nanoparticles.

Besides this, one more band gap is suggested to be present in the ZnO coated nanoparticles which is obtained at around 3.5 eV as shown in the Fig. 13b. So, we have observed an approximate band gap range from 3.5 to 3.8 eV because of different particle size (25–30 nm) of synthesized nanoparticles. The increase in band gap energy results in high energy required to eject an electron from valence band to conduction band. The energy stretch is extremely constructive for optical devices as it is easier to build laser on a material which has discrete energy of states rather than on a material which has broad continuum. This achieved increase in band gap energy is useful for the UV lasers. Also the tunability of energy band gap can be used to design light sources and detectors for particular use [64]. For the discrete energy levels formed with decrease in particle size, third order optical nonlinearities are observed, which can be used in optical switches, waveguides etc. [65]. Further, the band gap variation with size dependence for nanoparticles may be utilized in industrial applications where Si can be replaced with metal oxide semiconductor ZnO in light emitting diodes.

4 Conclusions

The wet chemical precipitation method has been used to synthesize the ligand directed (or modified) semiconductor

ZnO nanoparticles. ZnO nanoparticles have been successfully synthesized using $Zn(NO_3).6H_2O$, NaOH in methanol at room temperature along with the ligand. Photoluminescence spectra showed a significant decrease in the intensity of visible emission for mixed donor ligand directed ZnO nanoparticles, which clearly proved the inactiveness of the dangling bonds and the defect states which otherwise are present on the ZnO surface. ZnO nanoparticles capped with an organic receptor showed blue shift (towards lower wavelength side) in the absorbance spectra due to strong quantum confinement effects. The high and tunable band gap energy achieved in synthesized mixed donor ligand directed ZnO nanoparticles can be used for the fabrication of LEDs, solar cells, lasers and detectors.

Acknowledgments The authors are thankful to IIT Ropar for providing the SEM, EDAX and DLS measurements and Panjab University for providing the PL, TEM and LC–MS mass facility. Authors also acknowledge the facilities provided by CSIO for necessary solid state UV–Vis and FTIR measurements.

References

1. Z.R. Tian, J.A. Voigt, J. Liu, B. Mckenzie, M.J. Mcdermott, M.A. Rodriguez, H. Konishi, H. Xu, Nat. Mater **2**, 821 (2003)
2. Z.L. Wang, J. Phys. Condens. Matter **16**, R829 (2004)
3. S. Kumar, V. Gupta, K. Sreenivas, Nanotechnology **16**, 1167 (2005)
4. V. Gupta, P. Bhattacharya, Y.I. Yuzuk, K. Sreenivas, R.S. Katiyar, J. Cryst. Growth **287**, 39 (2006)
5. D. Bera, L. Qian, T.-K. Tseng, P.H. Holloway, Materials **3**, 2260–2345 (2010)
6. J. Xu, D.H. Cui, B.A. Lewis, A.Y. Wang, S.Y. Xu, M. Gerhold, IEEE Photonics Technol. Lett. **17**, 2008–2010 (2002)
7. S. Coe, W.K. Woo, M. Bawendi, V. Bulovic, Nature (London) **420**, 800–803 (2002)
8. S. Chaudhary, M. Ozkan, W.C.W. Chan, Appl. Phys. Lett. **84**, 2925–2927 (2004)
9. W.K. Bae, J. Kwak, J. Lim, D. Lee, M.K. Nam, K. Char, C. Lee, S. Lee, Nanotechnology **20**, 075202 (2009)
10. J.M. Caruge, J.E. Halpert, V. Bulovic, M.G. Bawendi, Nano Lett. **6**, 2991–2994 (2006)
11. J. Lee, V.C. Sundar, J.R. Heine, M.G. Bawendi, K.F. Jensen, Adv. Mater. **12**, 1102 (2000)
12. J. Lim, S. Jun, E. Jang, H. Baik, H. Kim, J. Cho, Adv. Mater. **19**, 1927–1932 (2007)
13. H.S. Chen, S.J.J. Wang, C.J. Lo, J.Y. Chi, Appl. Phys. Lett. **86**, 131905 (2005)
14. H.S. Chen, C.K. Hsu, H.Y. Hong, IEEE Photonics Technol. Lett. **18**, 193–195 (2006)
15. S. Nizamoglu, T. Ozel, E. Sari, H.V. Demir, Nanotechnology **18**, 065709 (2007)
16. D.M. Yeh, C.F. Huang, Y.C. Lu, C.C. Yang, Appl. Phys. Lett. **92**(09112), 1–3 (2008)
17. S.C. Lin, Y.L. Lee, C.H. Chang, Y.J. Shen, Y.M. Yang, Appl. Phys. Lett. **90**, 143517 (2007)
18. O. Niitsoo, S.K. Sarkar, C. Pejoux, S. Ruhle, D. Cahen, G. Hodes, J. Photochem. Photobiol. A **181**, 06–313 (2006)
19. Y.L. Lee, Y.S. Lo, Adv. Func. Mater. **19**, 604–609 (2009)
20. A. Zaban, O.I. Mimic, B.A. Gregg, A.J. Nozik, Langmuir **14**, 3153–3156 (1998)
21. L.J. Diguna, Q. Shen, J. Kobayashi, T. Toyoda, Appl. Phys. Lett. **91**(023116), 1–3 (2007)
22. D. Bera, L. Qian, P.H. Holloway, *Information Healthcare* vol 191 (New York, NY, USA, 2009)
23. A.M. Smith, X.H. Gao, S.M. Nie, Photochem. Photobiol **80**, 377–385 (2004)
24. R.E. Bailey, A.M. Smith, S.M. Nie, Physica E **25**, 1–12 (2004)
25. J. Bang, H. Yang, P.H. Holloway, Nanotechnology **17**, 973–978 (2006)
26. E. Kucur, W. Bucking, R. Giernoth, T. Nann, J. Phys. Chem. B **109**, 20355–20360 (2005)
27. O. Madelung (ed.), *Data in Science and Technology: Semiconductors* (Springer, Berlin, 1992)
28. J.B. Baxter, E.S. Aydil, Sol. Energy Mater. Sol. Cells **90**, 607 (2006)
29. K.H. Kim, K. Utashiro, Y. Abe, M. Kawamura, Materials **7**, 2522 (2014)
30. H. Kim, A. Pique, J.S. Horwitz, H. Murata, Z.H. Kafafi, C.M. Gilmore, D.B. Chrisey, Thin Solid Films **377**, 798 (2000)
31. S.N. Bai, T.Y. Tseng, J. Appl. Phys. **74**, 695 (1993)
32. O. Kluth, B. Rech, L. Houben, S. Wieder, G. Schope, C. Beneking, H. Wagner, A. Loffl, H.W. Schock, Thin Solid Films **351**, 247 (1999)
33. M. Aslam, V.A. Chaudhary, I.S. Mulla, S.R. Sainkar, A.B. Mandale, A.A. Belhekar, K. Vijayamohanan, Sens. Actuators A-phys. **75**, 162 (1999)
34. F. Pan, C. Song, X.J. Liu, Y.C. Yang, F. Zeng, Mater. Sci. Eng., R **62**, 1 (2008)
35. S.J. Pearton, C.R. Abernathy, D.P. Norton, A.F. Hebard, Y.D. Park, L.A. Boatner, J.D. Budai, Mater. Sci. Eng. R **40**, 137 (2003)
36. P.K. Stoimenov, R.L. Klinger, G.L. Marchin, K.J. Klabunde, Langmuir **18**, 6679–6686 (2002)
37. L. Fu, Y. Liu, B. Han, P. Hu, L. Cao, D. Zhu, Adv. Mater. **17**, 217–221 (2005)
38. V. Bojinov, N. Georgiev, J. Univ. Chem. Technol. Metall. **46**, 3 (2011)
39. A.V. Dijken, E.A. Meulenkamp, D. Vanmaekelbergh, A. Meijerink, J. Phys. Chem. B **104**, 1715 (2000)
40. M. Šćepanović, M. Grujić-Brojčin, Z. Dohčević-Mitrović, Z.V. Popović, J. Phys. Conf. Ser. **253**, 012015 (2010)
41. J. Han, P.Q. Mantas, A.M.R. Senos, J. Eur. Ceram. Soc. **22**, 49 (2002)
42. L. Schmidt-Mende, J.L. MacManus-Driscoll, Mater. Today **10**, 40 (2007)
43. C.L. Du, Z.B. Gu, M.H. Lu, J. Wang, S.T. Zhang, J. Zhao, G.X. Cheng, H. Heng, Y.F. Chen, J. Appl. Phys. **99**, 123515 (2006)
44. R.C. Wang, C.P. Liu, J.L. Huang, S.J. Chen, Appl. Phys. Lett. **87**, 053103 (2005)
45. H.T. Ng, B. Chen, J. Li, J.E. Han, M. Meyyappan, J. Wu, S.X. Li, E.E. Haller, Appl. Phys. Lett. **82**, 2023 (2003)
46. L. Huang, S. Wright, S. Yang, D. Shen, B. Gu, Y. Du, J. Phys. Chem. B **108**, 19901 (2004)
47. F. Wang, Z. Ye, D. Ma, L. Zhu, F. Zhuge, J. Cryst. Growth **274**, 447 (2005)
48. S.M. Abrarov, Sh.U. Yuldashev, T.W. Kim, S.B. Lee, Y.H. Kwon, T.W. Kang, Opt. Commun. **250**, 111 (2005)
49. Z. Chen, N. Wu, Z. Shan, M. Zhao, S. Li, C.B. Jiang, M.K. Chyu, S.X. Mao, Scr. Mater. **52**, 63 (2005)
50. P. Chandrasekaran, G. Viruthagiri, N. Srinivasan, J. Alloy. Compd. **540**, 89 (2012)
51. K. Sowri Babu, A. Ramachandra Reddy, K. Venugopal Reddy, Mater. Res. Bull. **49** 537–543 (2014)
52. S.B. Rana, V.K. Bhardwaj, S. Singh, A. Singh, N. Kaur, J. Mater. Sci. Mater. Electron. **24**, 20 (2013)
53. Y.H. Tong, Y.C. Liu, S.X. Lu, L. Dong, S.J. Chen, Z.Y. Xiao, J. Sol-Gel. Sci. Technol. **30**, 157 (2004)

54. X.W. Du, Y.S. Fu, J. Sun, X. Han, J. Liu, Semicond. Sci. Technol. **21**, 1202 (2006)
55. Y. Harada, S. Hashimoto, Phys. Rev. B **68**, 045421 (2003)
56. L.Y.L. Wu, A.I.Y. Tok, F.Y.C. Boey, X.T. Zeng, X.H. Zhang, IEEE Trans. Nanotechnol. **6**, 497–503 (2007)
57. S. Kaur, A. Kaur, N. Kaur, Mater. Lett. **100**, 19 (2013)
58. A. Sahai, N. Goswami, Ceram. Int. **40**, 14569–14578 (2014)
59. Y. Jiang, X.M. Meng, J. Liu, Z.Y. Xie, C.S. Lee, S.T. Lee, Adv. Mater. **15**, 323 (2003)
60. Y. Jiang, X.M. Meng, J. Liu, Z.R. Hong, C.S. Lee, S.T. Lee, Adv. Mater. **15**, 1195 (2003)
61. S. Monticone, R. Tufeu, A.V. Kanaev, J. Phys. Chem. B **102**, 2854 (1998)
62. J. Cao, J. Yang, L. Yang, M. Wei, B. Feng, D. Han, L. Fan, B. Wang, H. Fu, J. Appl. Phys. **112**, 014316 (2012)
63. G.C. Yi, C. Wang, W.I. Park, Semicond. Sci. Technol. **20**(4), 22 (2005)
64. K. Sattler, *Handbook of Thin Films Materials*, Volume **5**, Nanomaterials and Magnetic Thin Films. (Academic, New York, 2002), pp. 61–97
65. B.L. Justus, R.J. Tonucci, A.D. Berry, Appl. Phys. Lett. **61**, 3152 (1992)